The FIRST experiment at GSI: Detector performances with a 400 MeV/u ^{12}C beam

Z. Abou-Haidar[p,x], C. Agodi[f], M.A.G. Alvarez[p], T. Aumann[a], F. Balestra[h,k], G. Battistoni[b], A. Bocci[p], T.T. Böhlen[v,w], A. Boudard[u], A. Brunetti[c,i], M. Carpinelli[c,m], G.A.P. Cirrone[f], M.A. Cortés-Giraldo[q], G. Cuttone[f], M. De Napoli[d], M. Durante[a], J.P. Fernández-García[q], C. Finck[r], M.I. Gallardo[q], B. Golosio[c,m], E. Iarocci[e,j], F. Iazzi[h,k], G. Ickert[a], R. Introzzi[h], D. Juliani[r], J. Krimmer[t], N. Kurz[a], M. Labalme[s], A. Lavagno[h,k], Y. Leifels[a], A. Le Févre[a], S. Leray[u], F. Marchetto[h], V. Monaco[h,l], M.C. Morone[i,n], D. Nicolosi[aa,f], P. Oliva[c,m], A. Paoloni[e], V. Patera[e,j], L. Piersanti[e,j], R. Pleskac[a], J.M. Quesada[q], N. Randazzo[d], F. Romano[f,o], D. Rossi[a], V. Rosso[y,z], M. Rousseau[r], R. Sacchi[h,l], P. Sala[b], A. Sarti[e,j], C. Scheidenberger[a], C. Schuy[a], A. Sciubba[e,j], C. Sfienti[f,w], H. Simon[a], V. Sipala[d,m], E. Spiriti[g], L. Stuttge[r], S. Tropea[f] H. Younis[h,k],

[a]GSI Helmholtzzentrum für Schwerionenforschung, Darmstadt, Germany
[b]Istituto Nazionale di Fisica Nucleare - Sezione di Milano, Italy
[c]Istituto Nazionale di Fisica Nucleare - Sezione di Cagliari, Italy
[d]Istituto Nazionale di Fisica Nucleare - Sezione di Catania, Italy
[e]Istituto Nazionale di Fisica Nucleare - Laboratori Nazionali di Frascati, Italy
[f]Istituto Nazionale di Fisica Nucleare - Laboratori Nazionali del Sud, Italy
[g]Istituto Nazionale di Fisica Nucleare - Sezione di Roma 3, Italy
[h]Istituto Nazionale di Fisica Nucleare - Sezione di Torino, Italy
[i]Istituto Nazionale di Fisica Nucleare - Sezione di Roma Tor Vergata, Italy
[j]Dipartimento di Scienze di Base e Applicate per l'Ingegneria, "La Sapienza" Università di Roma, Italy
[k]Dipartimento di Fisica, Politecnico di Torino, Italy
[l]Dipartimento di Fisica, Università di Torino, Italy
[m]Università di Sassari, Italy
[n]Dipartimento di Biopatologia e Diagnostica per Immagini, Università di Roma Tor Vergata, Italy
[o]Centro Studi e Ricerche e Museo Storico della Fisica "Enrico Fermi", Roma, Italy
[p]CNA, Sevilla, Spain
[q]Departamento de Física Atómica, Molecular y Nuclear, University of Sevilla, 41080-Sevilla, Spain
[r]Institut Pluridisciplinaire Hubert Curien, Strasbourg, France
[s]LPC-Caen, ENSICAEN, Université de Caen, CNRS/IN2P3, Caen, France
[t]IPN-Lyon, Université de Lyon, Université Lyon 1, CNRS/IN2P3, Villeurbanne, France
[u]CEA-Saclay, IRFU/SPhN, Gif sur Yvette Cedex, France
[v]European Organization for Nuclear Research CERN, Geneva, Switzerland
[w]Medical Radiation Physics, Karolinska Institutet and Stockholm University, Stockholm, Sweden
[x]Universität Mainz Johann-Joachim-Becher, Mainz, Germany
[y]Dipartimento di Fisica, Università di Pisa, Italy
[z]Istituto Nazionale di Fisica Nucleare - Sezione di Pisa, Italy
[aa]Dipartimento di Fisica, Università di Catania, Italy

Abstract

FIRST (Fragmentation of Ions Relevant for Space and Therapy) is an experiment aimed at the measurement of double-differential cross sections, with respect to kinetic energy and scattering polar angle, of nuclear fragmentation processes in the energy range between 100 and 1000 MeV/u. The experiment was performed with the SIS accelerator at GSI (Darmstadt, Germany). During August 2011 a first set of data was collected using a 400 MeV/u ^{12}C ion beam on carbon and gold targets. We present a description of the experimental apparatus and some preliminary results from the data acquisition and from the data analysis.

1 Introduction

Hadron therapy has well known advantages with respect to conventional radiation therapy using photons. The ion beam energies can be chosen in such a way that the Bragg peak, the sharp peak of the released dose at the end of the ion range, falls inside the tumour, while sparing surrounding normal tissues. Compared to proton therapy, hadron therapy using ^{12}C beams has further advantages, among

these are a sharper lateral dose fall-off and a higher potential to treat radioresistant tumours due to its increased linear energy transfer (LET) at the end of the particle range. However, since the secondary fragments produced by the nuclear interactions of the beam with the tissue significantly contribute to the absorbed dose [1], fragmentation effects cannot be neglected. Currently, treatment planning systems for hadron therapy are generally based on deterministic codes for dose calculations which are relatively fast [2, 3]. These deterministic dose engines are often benchmarked against Monte Carlo simulations in order to test and improve their accuracy [4, 5]. The predictions of various theoretical models for the fragmentation process differ up to an order of magnitude for double-differential quantities (in energy and angle). Several measurements were made in the past of fragment yields and total cross sections (for a review see [6]), but double-differential cross section (DDCS) measurements are scarce. Accurate knowledge of fragmentation cross sections would also be important in the field of radiation protection in space missions. Recently, NASA completed a large database of nuclear fragmentation measurements [7] and observed that there are ion types and kinetic energy ranges where such measurements are missing. In particular, DDCS measurements for light ions in the energy range of interest for hadron therapy applications are lacking. The FIRST experiment is aimed at filling some of this lacking knowledge by measuring DDCS for light ions in the kinetic energy range between 100 and 1000 MeV/u.

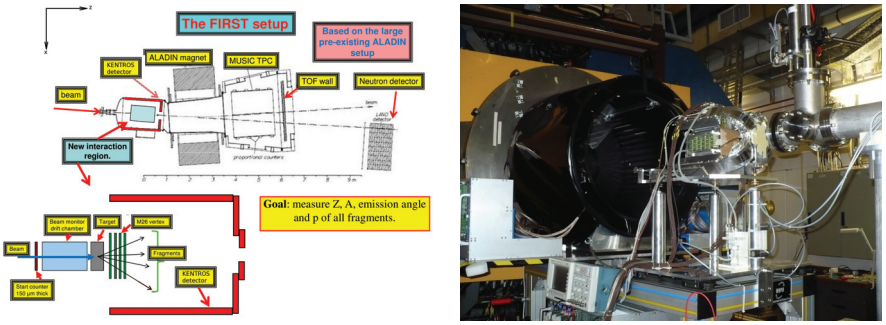

(a) (b)

Fig. 1: (a) Layout of the FIRST experiment with expanded interaction region. (b) The FIRST Interaction Region detectors during the installation.

2 Experimental setup

A detailed description of the experimental apparatus is reported in ref. [8]. Here only a short description will be given. A schematic layout of the FIRST experimental setup is shown in Fig. 1(a). The interaction region, shown in the enlarged portion of Fig. 1(a) and in the picture of Fig. 1(b), is composed of small area detectors that surround the target, before the ALADiN horizontal bending magnet. All these detectors have been specifically designed and built for this experiment. Following the beam path:

- the Start Counter [9] measures the starting time for the time-of-flight measurement. The active part of this detector is an EJ-228 fast scintillator foil (52 mm diameter, 250 μm thick). The scintillation signal is driven by four optical fibre bundles to four fast photomultipliers (Hamamatsu H10721-201);
- the Beam Monitor [9] measures the incoming ion direction and the impact point on the target. It consists of a drift chamber filled by an Ar-CO_2 80%-20% gas mixture and is composed of 36 sensing wires, arranged in six planes perpendicular to the beam, with the wires oriented alternatively in the horizontal and in the vertical direction;
- the Vertex Detector measures the tracks of charged particles originating from the target. It is based on the MIMOSA-26 silicon pixel sensor [10], which features an active area of $21.2 \times 10.6\,\mathrm{mm}^2$ segmented in 1152×576 pixels, with a 18.4 μm pitch. The layout of the detector (see Fig. 5(b)) is composed of four planes of about $2 \times 2\,\mathrm{cm}^2$ area, each plane being made of two partially overlapping MIMOSA-26 detectors spaced by 3 mm and with the long side oriented vertically. It

can measure tracks with an angular resolution of about 0.3 degrees up to polar angles of about 40 degrees;
- the KENTROS (Kinetic ENergy and Time Resolution Optimized on Scintillator) detector measures the time of flight and energy release of fragments with polar angles between about 5 degrees and 90 degrees. These measurements are used to identify the particle charges and to evaluate their kinetic energy. The KENTROS detector is divided in three subdetectors: a small endcap, which detects fragments with polar angles between 5 and 15 degrees, a big endcap for polar angles between 15 and 37 degrees, and a barrel for polar angles between 37 and 90 degrees. Each subdetector is composed of EJ-200 fast plastic scintillator modules. The scintillation signal is driven by plexiglass light guides to AvanSiD Silicon PhotoMultipliers (SiPM) with an active area of $4 \times 4\,\mathrm{mm}^2$. The SiPM signal is read by custom readout boards, with individual supply voltage control, signal amplification, reshaping and splitting to QDCs and to TDCs.

Behind the ALADiN bending magnet, large area detectors inherited from previous experiments were used. Following the beam path:

- the TP-MUSIC IV (Time Projection MUltiple Sampling Ionization Chamber) detector is a time projection chamber that measures the tracks of charged particles which exit the ALADiN magnet. The active volume is filled with a P10 (Ar-CH_4 90%-10%) gas mixture. It is divided in two symmetric parts by a central vertical cathode plane. The track projections on the non-bending (yz) plane[1] are determined by proportional counters located on the opposite sides of the detector, while the track projections on the horizontal bending (xz) plane are evaluated by measuring the ionization electron drift time from the track to the proportional counters. The readout is based on 14-bit FADC boards which digitize the signals coming directly from the preamplifiers. The MUSIC IV detector is able to measure with high efficiency and high resolution the charge and momentum of ions from He up to Au [11];
- the TOFWALL [12] measures the arrival time, energy release and impinging position of the fragments produced with polar angles smaller than about 6.5 degrees. It is composed of two layers, each made of 12 modules. Each module is composed of 8 BC-408 plastic scintillator slats, 110 cm long, 2.5 cm wide and 1 cm thick, oriented in the vertical direction. Each slat is read on both ends by two R3478 Hamamatsu photomultipliers. The signal is split and read out by Fastbus QDCs and by TDCs for charge and time measurements, respectively;
- the Large Area Neutron Detector (LAND) [13] is a large scintillation detector, having an active volume of about $2 \times 2 \times 1\,\mathrm{m}^3$, specifically designed for neutron detection. It is composed of 200 paddles having a volume of $200 \times 10 \times 10\,\mathrm{cm}^3$. Each paddle is made of 10 sheets of scintillator separated by sheets of iron. The scintillation light is collected on both ends of the paddles by stripe light guides, which drive it to the photomultipliers. The difference in the arrival times of the two signals is used to localize the position where the neutron interacts with the scintillator material, while the mean time is used to evaluate the neutron arrival time.

3 The first data taking at the GSI laboratory

The FIRST experiment was instrumented at the GSI laboratories in Darmstadt, and a first set of data was collected in 2011 between July and August. A total number of about 37 million events were collected and grouped in about 250 runs. Most of these measurements (about 32 million events) were made using a 400 MeV/u ^{12}C beam impinging on a 8 mm thick carbon target, while the remaining 5 million events were collected using a 5 mm thick gold target. Additional runs with special detector and target conditions were also taken for calibration and alignment purposes. The data acquisition was developed using the framework of the GSI Multi Branch System (MBS) [14]. This system can handle all the readout electronics standards (FASTBUS, CAMAC and VME) used in the experiment. Each readout crate was equipped with a trigger module connected through a single trigger bus to distribute the trigger and dead-time signals and to ensure event synchronization. The trigger signals from different detectors were fed into a programmable coincidence module where a logical combination of the signals could be used to produce the global trigger decision. Basically, this decision was based on an unbiased trigger provided

[1] The right-handed coordinate system used in this paper has the z axis pointing in the beam direction, the x axis pointing horizontally and the y axis pointing upwards. Polar and azimuthal angles are defined with respect to the z direction.

by the Start Counter. Other pre-scaled triggers with logical combinations of the Start Counter with other detectors were used for efficiency and calibration studies.

4 Detector performance

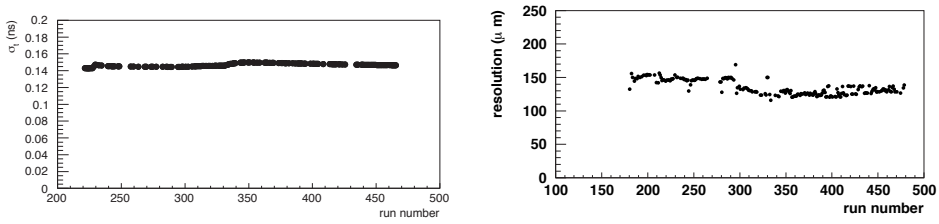

(a) (b)

Fig. 2: (a) Standard deviation of the time difference between pairs of Start Counter PMTs as a function of the run number. (b) Track spatial resolution of the Beam Monitor as a function of the run number.

The Start Counter efficiency was measured by using the unbiased sample of events triggered with the forward scintillator. It was found to be well above 99% in each of the runs even when requiring the coincidence of all the 4 PMTs, thus providing an indication of the high quality of the light collection system. The time resolution was determined by means of a gaussian fit of the distribution of the time difference between pairs of PMTs. The resulting sigma was in all runs better than 150 ps, as shown in Fig. 2(a). The time resolution, estimated as the standard deviation of the time difference between pairs of PMT divided by $\sqrt{2}$, is around 100 ps.

The performance of the Beam Monitor was also stable, as shown in Fig. 2(b). The space time relations used in the BM track reconstruction have been calibrated on a dedicated test beam [9] on a carbon beam of 80 MeV/u, with the same gas mixture at different high voltages. While the use of those calibrations is somewhat suboptimal, since they were obtained for carbon ions at a different energy, the results obtained are not far from the expected values: O(100 μm) [9]. Figure 2(b) shows that a track spatial resolution of 130-160 μm was achieved for all the C-C runs which is in agreement with the expected performances for the BM detector. This resolution corresponds to the standard deviation of the gaussian fit to the distribution of the difference between the hit and reconstructed track coordinates. The Beam Monitor measurement of the beam spot size, a Gaussian distributed circular spot of 1.3 mm σ was found to be in very good agreement with measurements performed by the Vertex Detector downstream of the target. The good performance of the Vertex Detector is evidenced in Fig. 3(a) where the number of clusters belonging to a track is shown for a single run. Although a minimum of 3 clusters are needed to build a track, the large majority of tracks incorporates one cluster in each of the four planes, indicating

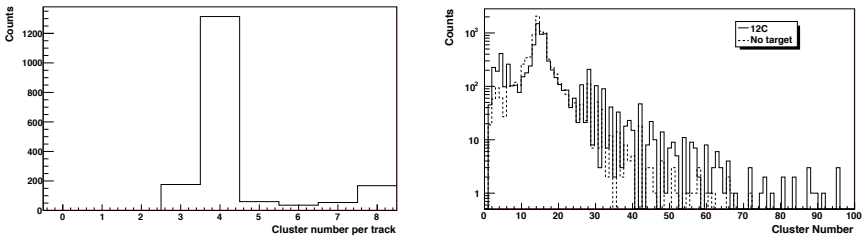

(a) (b)

Fig. 3: (a) Number of clusters per track in the Vertex Detector for ^{12}C on carbon run. (b) Number of pixels per cluster in the Vertex Detector for a run with the carbon target (solid line) and for a run without the target (dashed line).

a good tracking performance of this detector. In addition, a class of tracks crossing the planes in the overlap region between the two sensors is shown which incorporates up to eight clusters. For the same run, the total number of clusters belonging to a track in each of the eight sensors where about equal for sensors on the left side as well as for sensors on the right side. From this evaluation the efficiencies of the sensors appear to be uniform, the difference in the absolute number of tracked clusters, between sensors on the left or on the right with respect to the beam, being due to the beam not impinging perfectly centred on the Vertex Detector. Fig. 3(b) represents the distribution of the number of pixels belonging to a cluster, both for a run with the carbon target and for a run without the target. As expected the distributions are similar for carbon, gold and no target, since most of the events are non-fragmented events (i.e. mostly carbon ions). In Fig. 4(a), a section of the KENTROS TDC counts distribution, obtained requiring the

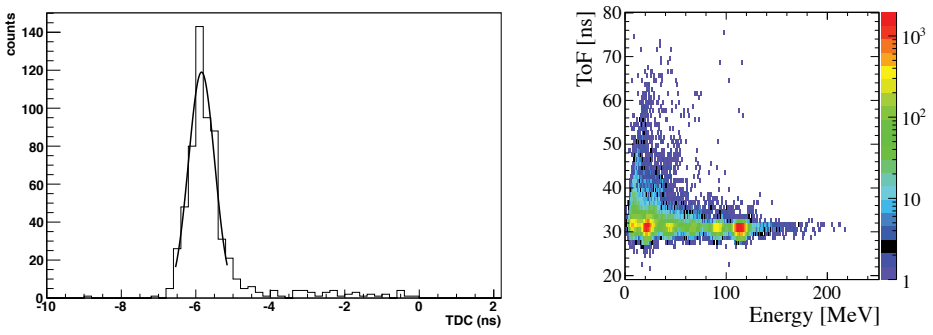

(a) (b)

Fig. 4: (a) TDC distribution on a Small Endcap module of the KENTROS detector, without time-walk correction, for QDC counts between 2200 and 2400. A gaussian fit to the peak of the histogram within $\pm 2\sigma$ shows a standard deviation of $\sigma \simeq 0.35$ ns. (b) ToF vs energy release ΔE_{TOF} in the TOFWALL. The six regions in the plot correspond to the ion fragments with $Z = 1, \ldots, 6$ from left to right.

related QDC counts to be consistent with the α particles energy release, was projected on the TDC axis. A gaussian fit to the peak of the histogram within $\pm 2\sigma$ shows a standard deviation of $\sigma \simeq 0.35$ ns. This value is influenced by the time-walk effect and by fluctuations of the scintillation signal transit time, which depends on the particle impact point on the detector module and will be corrected using the global track reconstruction information. Therefore, the standard deviation obtained by the fit should be regarded as an upper limit for the time resolution in our experimental conditions. The time of flight and the energy release, combined with the information on the tracks reconstructed by the Vertex Detector, will be used to evaluate the fragment kinetic energy. For the TOFWALL detector, the length of each slat (110 cm) requires to combine the values of the TDCs at both ends as average and the values of the ADCs as product, in order to cancel the dependence of the one-side measurement on the impact point. We shall denote the difference between the average time value of the TDCs and the time measured by the Start Counter as ToF; this quantity is related to the time of flight by a time offset to be determined individually for each slat. Similarly the square root of the ADCs product, converted to particle energy lost in the slat, is denoted as ΔE_{TOF}. Some special runs with no target and with the magnetic field of the ALADiN continuously varied were dedicated to the calibration of the TDCs and ADCs. The ToF calibration for the ^{12}C ion beam at 400 MeV/u, over all slats of the TOFWALL was tuned with a time offset chosen in each slat such that the ToF distribution for non-fragmented carbon ions at 400 MeV/u was centred at $\sim$32 ns. An upper limit for the real time resolution σ of 0.5 ns, was obtained, to be compared with a minimum time of $\sim$28 ns spent by the fastest fragments to reach the TOFWALL. The scatter plot of ToF versus ΔE_{TOF} measured by a single slat in all runs with carbon as target and a beam energy of 400 MeV/u is shown in Fig. 4(b). The six separated regions which appear in the plot correspond to ion fragments $Z = 1, \ldots, 6$ from left to right. They suggest a good charge identification capability of this detector. The time of flight information will be used together with the global track reconstruction to evaluate the kinetic energy of the fragments. The tracking performance of the detectors of the Interaction Region:

Beam Monitor, Vertex Detector and KENTROS, are easily monitored by means of a 3D event display, as shown in Figs. 5(a) and 5(b).

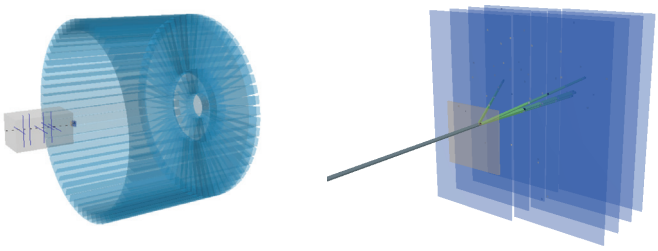

(a) (b)

Fig. 5: (a) Interaction Region event display. (b) Vertex Detector event display.

5 Conclusion

The FIRST experiment was designed for the measurement of nuclear fragmentation cross sections, double differential with respect to kinetic energy and scattering polar angle, for light ions in the range between 100 and 1000 MeV/u. The experiment was instrumented at the GSI laboratory and a first data acquisition took place during summer 2011. About 37 million events were acquired using a 400 MeV/u ^{12}C beam impinging on carbon (32 M) and gold (5 M) targets. The data analysis is still in progress. However from the preliminary analysis the measured values of the detector resolutions and the quality of the data match perfectly the expected performance.

Acknowledgement

We would like to acknowledge M. Arba, L. La Delfa and M. Tuveri (INFN Sez. Cagliari), M. Anelli, S. Cerioni, G. Corradi, D. Riondino and R. Rosellini (INFN, LNF), M. Capponi and A. Iaciofano (INFN, Sez. Roma3) for the technical design and mechanical work on the Interaction Region, and Filippo Bosi (INFN Sez. Pisa) for his help and suggestions. We also acknowledge Dr. Håkan T. Johansson for the invaluable help in setting up the trigger. This work has been supported by the European Community FP7 - Capacities, contract ENSAR n° 262010 and People PITN-GA-2008-215840-PARTNER. This work was also supported by Junta de Andaluca and the Spanish Ministerio de Ciencia e Innovación Contracts P07-FQM-02894, FIS2008-04189 and FPA2008-04972-C03. Finally some of the authors would like to thank CNRS-In2p3 for the support.

References

[1] E. Haettner *et al.*, Radiat. Prot. Dosim. **122**(1-4) (2006) 485.

[2] M. Krämer and M. Durante, Eur. Phys. J. D **60**(1) (2010) 195.

[3] L. Sihver and D. Mancusi, Radiat. Meas. **44**(1) (2009) 38.

[4] K. Parodi *et al.*, Proc. 12th Int. Conf. on Nucl. Reac. Mechan. (Varenna, Italy, 15th-19th June 2009), available at http://cdsweb.cern.ch/record/1238366/files/p509.pdf.

[5] T. T. Böhlen *et al.*, Phys. Med. Biol. **55**(19) (2010) 5833.

[6] D. Schardt *et al.*, Rev. Mod. Phys. **82**(1) (2010) 383.

[7] J.W. Norbury and J. Miller, 47th NCRP Annual Meeting, Bethesda, MD (2011) 24.

[8] R. Pleskac *et al.*, Nucl. Instrum. Meth. *A678* (2012) 130.

[9] Z. Abou-Haidar *et al.*, J. Instrum. **7** (2012) P02006.

[10] http://www.iphc.cnrs.fr/-CMOS-ILC-.html

[11] C. Sfienti *et al.*, "Isotopic dependence of the nuclear caloric curve", Phys. Rev. Lett. **102**(15) (2009) 152701.

[12] A. Schüttauf *et al.*, Nucl. Phys. A **607**(4) (1996) 457.

[13] K. Boretzky *et al.*, Phys. Rev. C **68**(2) (2003) 243171.

[14] H.G. Essel and N. Kurz, IEEE TNS **47**(2) (2000) 337.